Electronic Supplementary Material (ESI) for Energy & Environmental Science.

Supplementary Information for

Investigation of a hybrid solar-redox scheme for liquid fuel and hydrogen coproduction

Feng He [a], James Trainham[b], Gregory Parsons[a], John S. Newman[b,c], and Fanxing Li*[a]

[a] *Department of Chemical and Biomolecular Engineering, North Carolina State University,*
911 Partners Way, Raleigh, NC 27695-7905, USA.
**Email: Fli5@ncsu.edu*

[b] *RTI International, 3040 E Cornwallis Road, Research Triangle Park, NC 27709-2194*

[c] *Department of Chemical Engineering, University of California, Berkeley, CA 94720-1462*

Metal Oxide Synthesis:

Lanthanum strontium ferrite ($La_{0.8}Sr_{0.2}FeO_{3-\delta}$ or LSF) supported Fe_3O_4 is used as the redox material, a.k.a. oxygen carrier, for water-splitting. The LSF support, which is an effective mixed ionic-electronic conductor, can inhibit the sintering of iron/iron oxides, thereby enhancing the redox activity and thermal stability of the iron oxide.[1,2] Fe_2O_3 is used as the precursor for Fe_3O_4. The oxygen carrier precursor contains 60 w.t.% Fe_2O_3 balanced with LSF. A solid-state reaction (SSR) method is used for oxygen carrier synthesis. Briefly speaking, a stoichiometric amount of precursors, i.e. iron oxide (Fe_2O_3, 99.9%, Noah Chemicals), La_2O_3 (99.9%, Aldrich), and $SrCO_3$ (99.9%, Noah Chemical), are weighed and mixed using a planetary ball-mill (XBM4X, Columbia International) for 6 hours. The solid mixture is then pelletized using a hydraulic press (YLJ-15T, MTI Corporation) under 7 to 8 MPa pressure. This is followed with annealing in air at 1200°C for 28 hours in a tube furnace (GSL-1500-X50, MTI Corporation). The resulting pellets are subsequently crushed and sieved into 75 to 300 μm for further characterization and testing. The as-prepared metal oxide obtained is composed of Fe_2O_3 and LSF. In order to obtain Fe_3O_4 phase, one cycle reduction with methane followed with steam regeneration is performed. Further details of the SSR method have been reported earlier.[1,2]

Experimental set up

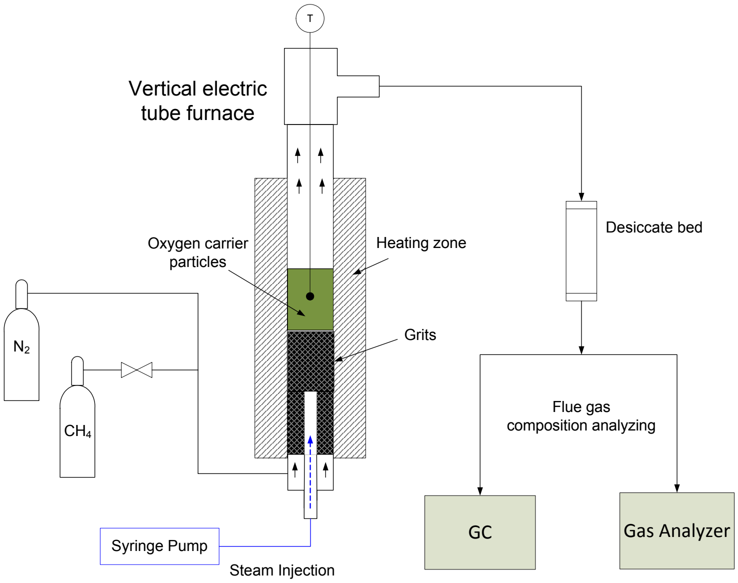

Fig. S1 Experimental setup for hybrid redox process test with Fe_2O_3-LSF particle.

Simulation assumptions

Aspen Plus is used in the present study to determine the reactor and process performances. Table S1 specifies the materials involved in the simulations. Since LSF is not available in the Aspen Plus database, SiC is used as the inert support in our simulations. It is noted that LSF support does not participate in the redox reaction to an appreciable extent. Replacement of LSF support with SiC will not affect the simulation results since the support material acts mainly as a heat carrier from a mass and energy balance standpoint. Aspen Plus modules, property methods, and physical property databanks are summarized in Table S2. PR-BM is selected as the property method in all the simulation modules except for steam cycles, where STEAM-TA method is used. Table S3 lists the key operating assumptions and parameters used in the process simulations.

Table S1 Specifications of the materials

Methane	HHV (higher heating value) 55.5 MJ kg^{-1}, LHV 50.0 MJ kg^{-1}
Concentrated solar energy input	52-62 MW[3-5]
Absorption efficiency for solar energy	80%[3,4,6]
Air	79% N_2, 21% O_2 by volume
Oxygen carrier	Fe_3O_4, SiC (inert)
Water	H_2O
H_2 product	Purity: >99.99%, Pressure: 6 MPa
Naphtha	C_6-C_{11}
Diesel	C_{12}-C_{18}

Table S2 Aspen Plus model setup

Overall setup	
Stream class	MIXCINC
Databank	COMBUST, INORGANIC, SOLIDS, PURE
Solid components	Fe, $Fe_{0.947}O$, Fe_3O_4, SiC, C
Property method	PR-BM, except STEAM-TA for steam cycles
Solution strategy	Sequential Modular
Unit operations models	
Reducer	Single-stage RGibbs; RGibbs
Oxidizer	Multi-stage RGibbs (moving bed); RGibbs
F-T Reactor	RStoic
Pressure changers	Pump, Compr, Mcompr
Heat exchangers	Heater, MheatX
Mixers/Splitters/Separators	Mixer/Fsplit/Sep/Flash2
Reducer	Single-stage RGibbs

Table S3 Key assumptions and simulation parameters in the Aspen Plus simulation

Parameter	Value
Ambient condition	*T* = 25 °C, *P* = 1 atm
Reaction assumptions	Except for Case III, all reactions reach equilibrium
Heat loss in the reactors	1% of the total thermal input
F-T catalyst	Cobalt
F-T reactor temperature and pressure	220 °C; 10 atm
F-T α parameter	0.873
CO per-pass conversion in the F-T reactor	80% (10 atm)
Pressure drop in the reducer and oxidizer	0.5 atm
Mechanical efficiency of pressure changers	1
Isentropic efficiency of steam turbines	0.85
Isentropic efficiency of air blowers and compressors	0.8
Heat Recovery Steam Generator	Pinch point: 15 ℃
PSA	5 atm pressure drop, 95% H_2 recovery
Compressor specifications	4 stage with intercooler at 40°C, Isentropic efficiency is 0.8
Steam turbine conditions	3-level Steam Cycle 12.4 MPa (HP inlet)/3.1MPa(IP inlet)/0.45MPa(LP inlet)/0.01MPa(LP outlet)

Key reactions in the hybrid solar-redox scheme

Key chemical reactions are given below. It includes methane conversion reactions in the reducer (A) and water-splitting reactions in the oxidizer (B).

Table S4 Key chemical reactions in the redox scheme

	Reactions	Free energy@900 °C kJ/mol
	Reducer (Methane conversion)	
A1.	$CH_4 + Fe_3O_4 \rightarrow CO + 2H_2 + 3FeO$	-78.3
A2.	$CH_4 + 4Fe_3O_4 \rightarrow CO_2 + 2H_2O + 12FeO$	-99.5
A3.	$CH_4 + 4FeO \rightarrow CO_2 + 2H_2O + 4Fe$	-49.9
A4.	$CH_4 + FeO \rightarrow CO + 2H_2 + Fe$	-65.9
A5.	$CO + Fe_3O_4 \rightarrow CO_2 + 3FeO$	-5.34
A6.	$CO + FeO \rightarrow CO_2 + Fe$	7.07
A7.	$H_2 + Fe_3O_4 \rightarrow H_2O + 3FeO$	-7.91
A8.	$H_2 + FeO \rightarrow H_2O + Fe$	4.49
A9.	$CO + H_2O \rightarrow CO_2 + H_2$	2.57
A10.	$CH_4 \rightarrow C + 2H_2$	-38.0
	Oxidizer (Water-splitting)	
B1.	$H_2O + Fe \rightarrow FeO + H_2$	-4.49
B2.	$H_2O + 3FeO \rightarrow Fe_3O_4 + H_2$	7.91
B3.	$H_2O + C \rightarrow CO + H_2$ (coke is formed in reducer)	-32.4
B4.	$2H_2O + C \rightarrow CO_2 + 2H_2$	-29.8

Product gas concentration from reducer as a function of time

While the real time methane conversion and syngas yield in the experiment are presented in the manuscript (Fig. 2), the corresponding product gases concentration as a function of time in the reducer is shown in Fig. S2.

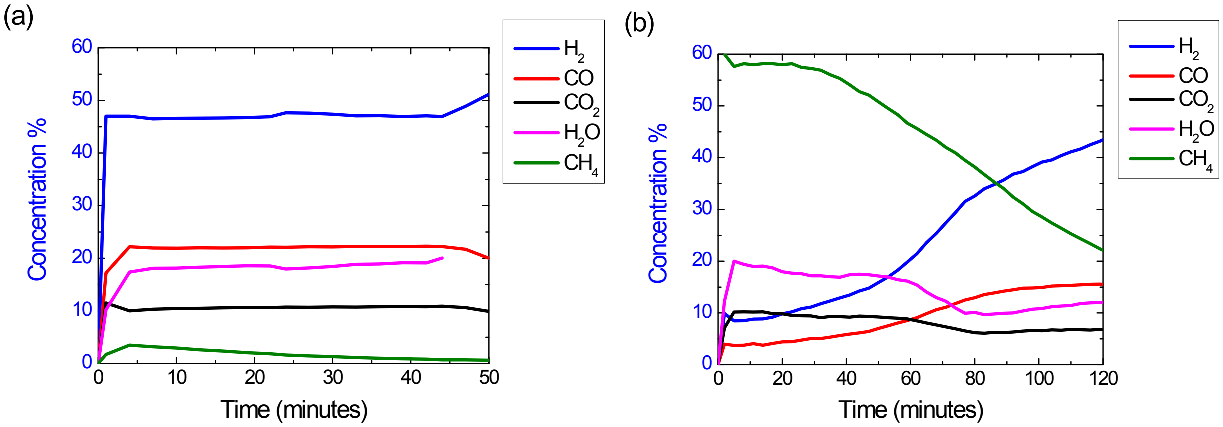

Fig. S2 Product gases concentration (N_2-free) as a function of time in the CH_4 oxidizing step. (a) 5th cycle fixed-bed (b) 5th cycle fluidized-bed.

Fe_3O_4-LSF reactivity in the reducing step

Reactivity study on Fe_3O_4-LSF is also conducted in a differential bed reactor system composed of a computer-controlled panel for gas mixing and delivery, a TGA (STARAM SETSYS Evolution) for redox reactions, and a quadrupole mass spectrometer (QMS, MKS Cirrus 2) for gaseous product analyses. In the experiment, 50 mg Fe_3O_4-LSF is heated to 900 °C at a rate of 50 °C/min. And then the reacting gas in injected at the temperature of 900 °C for 10 minutes. Total gas flow rate is maintained at 300 ml/min. Concentrations of the reactive gases (CH_4) is fixed at 10%. Helium is used as the carrier gas. Product distributions and catalyst selectivity towards syngas are determined using the QMS. TGA experiments are designed to obtain confirmation for the Fe_3O_4-LSF particle activity to react with methane. At about 0.9 minutes during the experiment, the average phase of iron oxides is FeO. The methane conversion and syngas yield are relatively low at the beginning of the experiment. Then, methane conversion rate and syngas yield increase significantly with time or increasing degree of iron oxide reduction. At approximately 5 minutes of CH_4 injection, coke starts to form based on the carbon mass balance calculation. It causes the H_2/CO molar ratio to exceed 2, where methane should be stopped to inhibit the coke formation. Coke formation is found to stop at between 5.8 and 6 minutes. At that point, no further conversion of methane is observed due to lack of active lattice oxygen and lack of coke formation. In an actual process, constant reduction and regeneration of the oxygen carrier will be implemented as in fixed/fluidized bed experiments. Fig. S3 summarizes the experimental results.

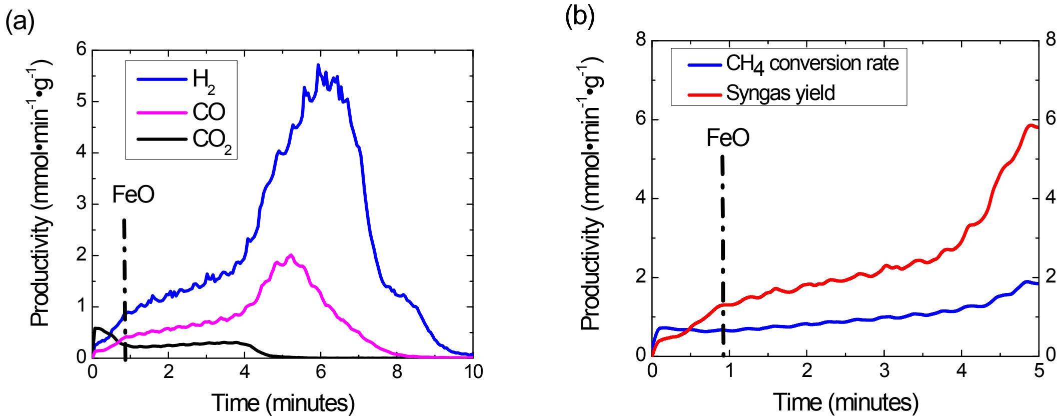

Fig. S3 Flue gas analysis of Fe_3O_4-LSF and CH_4 reaction at 900 °C (a) flow rates of product gases (b) methane conversion rate and syngas yield.

X-ray powder diffraction results

X-ray powder diffraction (XRD) tests are carried out for spent oxygen carriers in both reduced and oxidized forms. The results are provided in Fig. S4. Both wustite and metallic iron are observed in the reduced sample whereas the majority of the iron phase in the regenerated sample is magnetite. Iron carbide phases are not identified in the reduced sample, indicating that amorphous carbon and/or carbon fiber may represent the dominant forms of carbon.

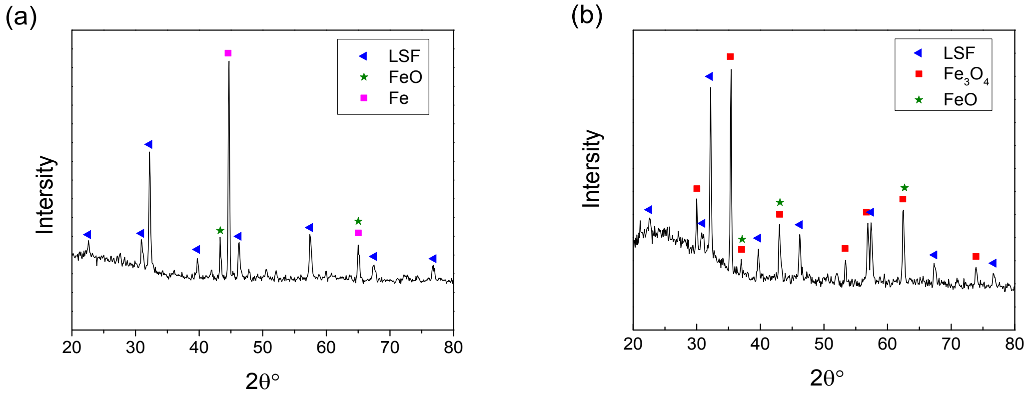

Fig. S4 XRD results of the (a) reduced; (b) oxidized OC particles.

Experimental results on multi-cyclic studies

7.5 to 20 grams of iron oxide particles are added on top of the SiC layer in the tubular reactor. In order to mimic the proposed hybrid redox scheme, the tests are carried out in two consecutive steps, i.e. methane partial oxidation and water-splitting. Both fixed-bed and fluidized-bed operation modes are tested. In typical fixed-bed experiments, the reactor is heated under N_2 flow of 15 ml/min. In fluidized-bed experiments, 600 ml/min of N_2 gas is provided during the heating stage to maintain fluidization of the Fe_3O_4-LSF particles. Once the desired temperature (900 °C unless otherwise specified) is reached, 15 ml/min of methane is introduced to the reactor. In order to inhibit excessive carbon formation from methane decomposition, methane injection is stopped when $H_2/(CO+CO_2)$ molar ratio exceeds 2. Water-splitting reaction is carried out after the residue gas from the methane oxidation step has been completely purged with N_2. The water-splitting reaction is initiated by steam injection. 50 ml/min (fixed-bed) or 600 ml/min (fluidized-bed) of N_2 is used as the internal standard. The reaction is stopped when H_2 concentration is below 0.1%. The aforementioned redox reactions are carried out for 5 cycles. And the results are shown in the Fig. S5. The CH_4 conversion, syngas yield and H_2/CO molar ratio is calculated for the reducing step, while the steam to H_2 conversion is calculated for the oxidizing step. Reproducible results are found among the various redox cycles.

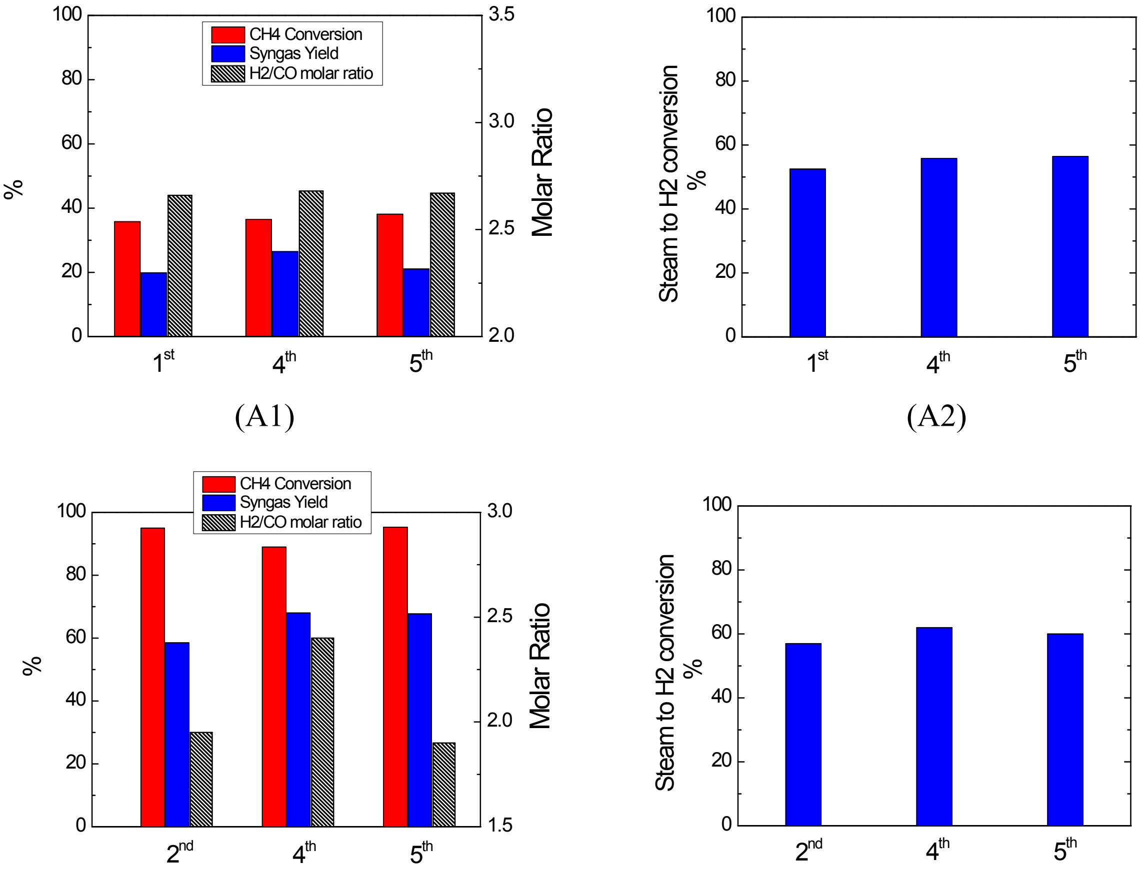

(B1) (B2)

Fig. S5 Experimental data from 5 redox cycles performance on (A) fluidized bed and (B) fixed bed.

Comparison of the oxygen carrier activity for energy conversion

The hybrid solar-redox process investigated in the current study represents an alternative scheme that converts methane and solar energy into separate streams of liquid fuels and hydrogen. Compared to the conventional solar water splitting scheme, solar-redox process has the advantages of multiple products and low reducing reaction temperature. In the present work, Lanthanum strontium ferrite ($La_{0.8}Sr_{0.2}FeO_{3-\delta}$ or LSF) supported Fe_3O_4 (60 wt%) is used as the redox oxygen carrier material. According to our experimental study, it is found 95% average methane conversion is achieved in the fixed-bed at 900 °C. Syngas with 2:1 H_2 and CO molar ratio, which is ideal for F-T synthesis, can be generated. Hydrogen with an overall purity in excess of 97% is generated in the subsequent water-splitting step. The water-splitting step also exhibits high steam to hydrogen conversion. In sum, the particle shows promising activity for solar redox process.

Kodama et al[7] studied an iron oxide supported on yttrium-stabilized zirconia (YSZ) at 1400 °C for the conventional solar water splitting scheme. Mixed oxides based ferrite materials with general formula of $M_xFe_{3-x}O_4$ (M = Mn, Co, Ni, Zn, Mg, etc.) has also been investigated as the alternative oxygen carrier.[8-11] $CoFe_2O_4$ and Al_2O_3 was tested in the isothermal redox cycles for H_2 generation.[12] The H_2 generation rates and oxygen carrier activities reported in their work are all in the same range. For comparison, we take the results of the Fe_3O_4/YSZ particle from Kodama et al., which is shown in Table S5. The product generation rate is calculated by the energy of the product (HHV based) per gram of the oxygen carrier particle and per reaction time. As indicated in Table S5, the Fe_3O_4/LSF used in the present work gives much higher H_2 generation rate. In addition, syngas is produced in the reducing step in the meantime. The total products generation rate is about 20 time more than conventional solar water splitting scheme by using the Fe_3O_4/LSF particle.

Table S5 Comparison of Fe_3O_4 particle activity in the hybrid solar-redox and water splitting scheme

	Peak H_2 generation rate $J\ g^{-1}\ min^{-1}$	Average H_2 generation rate $J\ g^{-1}\ min^{-1}$	Syngas generation $J\ g^{-1}\ min^{-1}$	Total product generation rate $J\ g^{-1}\ min^{-1}$
Ref[7]	6.3	3.2	NA	3.2
Our work	49.8*	49.8	12.9	62.7

* H_2 generation close to steady state achieved in our work

The Aspen Plus® process configuration

The ASPEN simulation model developed for the hybrid solar-redox process operating at low pressure for the redox reactions is shown in Fig. S6. It includes: (1) the redox section which has reducer and oxidizer; (2) the F-T synthesis section where consists of the F-T reactor, upgrader and syngas compressor; (3) the power generation section which has steam turbines and HRSG; (4) the product purification section. As the process feedstock, methane is fed into the reducer, where it is partially oxidized by the oxygen carrier into syngas. In order to compensate the heat required for the endothermic methane oxidation reaction, solar energy is provided by direct irradiation. A methane processing capacity of 8 tonne/hr is assumed for all cases. Such a capacity, which requires solar input of approximately 60 MW_{th}, allows for integration with existing concentrated solar thermal systems,[1-3] Syngas produced by methane partial oxidation in the reducer is used as the feedstock for F-T synthesis. Byproducts from the F-T reactor, upgrader, and PSA units are recycled to the reducer to produce additional syngas. Besides syngas, the reducer generates reduced oxygen carrier particles which are transported to the oxidizer for water-splitting. The H_2 generated from the water-splitting or steam-iron reaction is cooled, cleaned, and compressed as the final product. The high temperature gaseous products from the reactors as well as the heat generated from the F-T reactor are directed to a Heat Recovery Steam Generator (HRSG) for (partial) heat reclamation. A 3-pressure level steam turbines system is used to generate power to satisfy parasitic energy requirements. The final products from the solar-redox process comprises high purity compressed H_2, liquid fuel and electricity.

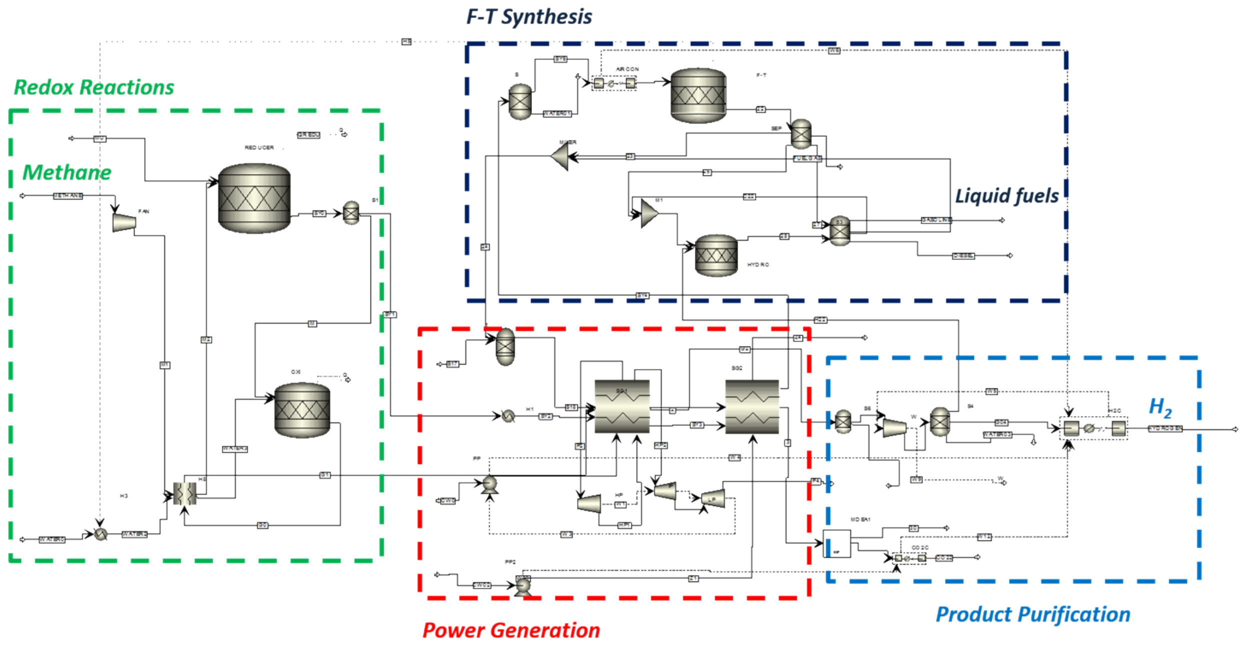

Fig. S6 ASPEN Plus® flowsheet of the hybrid solar-redox process operating at low pressure for the redox reactions

Process material balance:

Table S6 shows the mass flow rate of the gaseous products from inlet and outlet of the key reactors in the hybrid solar-redox process. The results are exported from Aspen Plus simulation of Case III.

Table S6 Key mass flow (kmol/hr) in the hybrid solar-redox process of Case III

	Feedstock of the reducer	After reducer	Fuel gas after F-T	Liquid fuel collector	After Oxidizer	After PSA
CO	0	304.0	65.9	0	4.8	0
CO_2	0	142.5	167.4	0	23.7	0
H_2	0	574.8	100.7	0	1016.4	965.6
H_2O	0	375.2	0	0	680.2	0
CH_4	500.0	25.0	26.7	0	0	0
C_2-C_4	0	0	3.9	0	0	0
C_5-C_{11}	0	0	0	10.9	0	0
C_{12}-C_{19}	0	0	0	9.4	0	0

Energy consumption in key unit operation steps:

The energy consumption and generation from key unit operations in the hybrid solar-redox process are given in Table S7. The results are exported from Aspen Plus simulation of Case III, where negative number represents energy consumption and positive number shows power generation.

Table S7 Energy consumption and generation from key unit operations in the hybrid solar-redox process of Case III

	Energy (MW)
Syngas compression	-4.49
PSA	-2.6
H_2 compression	-4.12
Total consumption	***-11.21***
Heat recovery	2.83
Flue gas combustion	11.88
Total generation	***14.71***
Net Power	**3.5**

References:

1. N. L. Galinsky, Y. Huang, A. Shafiefarhood, and F. Li, *ACS Sustainable Chem. Eng.*, 2013, **1**, 364–373.
2. A. Shafiefarhood, N. Galinsky, Y. Huang, Y. Chen, and F. Li, *ChemCatChem,* 2014, **6**, 790-799.
3. A. Steinfeld, *Int. J. Hydrog. Energy*, 2002, **27**, 611–619.
4. T. Kodama, *Prog. Energy Combust.*, 2003, **29**, 567–597.
5. S. Möller, D. Kaucic, and C. Sattler, *J. Sol. Energy Eng.*, 2005, **128**, 16–23.
6. M. Roeb, A. G. Konstandopoulos, A. Steele, P. Stobbe, et al, *J. Sol. Energy Eng.*, 2005, **128**, 125–133.
7. T. Kodama, Y. Nakamuro, and T. Mizuno, *J. Sol. Energy Eng.*, 2004, **128**, 3–7.
8. Y. Tamaura, A. Steinfeld, P. Kuhn, and K. Ehrensberger, *Energy*, 1995, **20**, 325–330.
9. T. Kodama, N. Gokon, and R. Yamamoto, *Sol. Energy*, 2008, **82**, 73–79.
10. J. R. Scheffe, J. Li, and A. W. Weimer, *Int. J. Hydrog. Energy*, 2010, **35**, 3333–3340.
11. M. Roeb, M. Neises, N. Monnerie, F. Call, H. Simon, C. Sattler, M. Schmücker, and R. Pitz-Paal, *Materials*, 2012, **5**, 2015–2054.
12. C. L. Muhich, B. W. Evanko, K. C. Weston, P. Lichty, X. Liang, J. Martinek, C. B. Musgrave, and A. W. Weimer, *Science*, 2013, **341**, 540–542.